LETTER Communicated by John Rinzel

Hybrid Integrate-and-Fire Model of a Bursting Neuron

Barbara J. Breen
bbreen@ece.gatech.edu
William C. Gerken
wgerken@ece.gatech.edu
Robert J. Butera, Jr.
rbutera@ece.gatech.edu
Laboratory for Neuroengineering, Schools of Physics, Electrical and Computer Engineering, and Biomedical Engineering, Georga Institute of Technology, Atlanta, GA 30332, U.S.A.

We present a reduction of a Hodgkin-Huxley (HH)–style bursting model to a hybridized integrate-and-fire (IF) formalism based on a thorough bifurcation analysis of the neuron's dynamics. The model incorporates HH-style equations to evolve the subthreshold currents and includes IF mechanisms to characterize spike events and mediate interactions between the subthreshold and spiking currents. The hybrid IF model successfully reproduces the dynamic behavior and temporal characteristics of the full model over a wide range of activity, including bursting and tonic firing. Comparisons of timed computer simulations of the reduced model and the original model for both single neurons and moderately sized networks ($n \leq 500$) show that this model offers improvement in computational speed over the HH-style bursting model.

1 Introduction

Endogenously bursting neurons have been the subject of intensive mathematical modeling and computer simulation. Because of the rich repertoire of biophysical mechanisms involved in bursting, mathematical models that attempt to reproduce these dynamics accurately can be complex. Conductance-based models of the *Aplysia* neuron R15, for example, may contain 12 or more state variables and over 50 parameters (Bertram, 1993; Butera, Clark, Canavier, Baxter, & Byrne, 1995; Canavier, Clark, & Byrne, 1991). Even the simplest reduced bursting models (Butera, Rinzel, & Smith, 1999a; Rinzel & Lee, 1987) still must include variables that evolve on two radically different timescales,—typically three to four orders of magnitude. The slow variables govern a slow oscillation in the membrane voltage that alternates between a silent state and an oscillatory state. The oscillatory state is characterized by the firing of action potentials governed by fast variables, and the periodic alternation between silence and spiking is referred to as bursting.

Computationally simpler models lend themselves more readily to simulation, analysis, and prediction. In general, efforts at simplification focus on reducing the complexity of bursting systems while maintaining a relationship between the model and experimentally measured quantities. Usually the system is separated into two subsystems, which characterize the fast and slow dynamics of the neuron. Some approaches seek to combine variables that evolve on similar timescales into an equivalent single variable (Kepler, Abbott, & Marder, 1992). Other approaches to simplifying bursting neuron models have included perturbation analysis (Rinzel, 1985, 1987), quantifying the effect of the firing of action potentials on the evolution of the slow variables (Smolen, Terman, & Rinzel, 1993; Baer, Rinzel, & Carillo, 1995; Butera, Clark, & Byrne, 1997) bifurcation analysis of the model to find membrane potential spike-frequency characteristics in terms of the slow variables (Ermentrout, 1994), and characterizing the interactions between the fast and slow subsystems via systematic manipulations of the model (Butera, Clark, & Byrne, 1996).

One of the simplest computational model neurons is the integrate-and-fire (IF). In the IF model (Lapicque, 1907), spike frequency and voltage baseline are controlled by a rule that dictates the resetting voltage V_{Reset} after the threshold voltage V_{Thresh} is crossed. This model captures certain fundamental features of the neuron such as the evolution of a subthreshold membrane voltage, the generation of a "spike event" when a given voltage threshold is crossed, and the return of membrane voltage to a baseline after the spike event. Adaptations of either V_{Thresh} and V_{Reset} have been shown to produce more complex behavior (Koch, 1999). More elaborate variants of IF models have incorporated the effects of Hodgkin-Huxley (HH)-style conductances by approximating the voltage-dependent rate constants and deriving piecewise analytic expressions for the gating variables (Destexhe, 1997).

In this study, we perform a bifurcation analysis of the reduced fast subsystem. From features of the bifurcation diagram, we derive functions for V_{Thresh} and V_{Reset} in terms of the single slow variable h. In addition, we use the bifurcation analysis to quantify the perturbational effects of the action potential on the slow variable. The net result is an HH-like formalism for the subthreshold currents and an IF formalism for the spiking currents, with the interactions between them fully described. While this approach has been pursued ad hoc by others (MacGregor, 1987; Smith, Cox, Sherman, & Rinzel, 2000; Hansel & Mato, 2003), here the interactions have been rigorously derived from an existing higher-order HH-type model.

2 Methods

Our single-cell analyses were accomplished with the software XPPAUT (Ermentrout, 2002), using the built-in CVODE integrator. Single-cell simulations for performance analysis were implemented in both the C program-

ming language using a fourth-order Rosenbrock semi-implicit extrapolation method stiff integrator (Press, Flannery, Teukolsky, & Vetterling, 1992) and in the NEURON (v. 5.4) simulation environment (Hines & Carnevale, 1997, 2000) using the built-in CVODE integrator. Network simulations were also implemented in NEURON. Threshold crossing detection and the handling of synaptic events were facilitated by NEURON's event-handling features.

The parameter fits in the computational performance section were implemented using the *fminsearch* command in MATLAB (Mathworks, Natick, MA), which implements the Nelder-Meld simplex direct search method. Performance timings were implemented on computers with Pentium III 800 MHz microprocessors and 1 Gb of RAM, running the Linux operating system.

We chose as our base model a three-variable HH formulation of respiratory bursting neurons in the pre-Bötzinger complex of mammals (Butera et al., 1999a),

$$C\frac{dV}{dt} = -I_{\mathrm{Na}}(V) - I_{\mathrm{NaP\text{-}h}}(V) - I_{\mathrm{K}} - I_{\mathrm{L}} + I_{\mathrm{app}} \tag{2.1}$$

$$I_{\mathrm{Na}} = g_{\mathrm{Na}} m_{\infty}^{3}(V)(1-n)(V - E_{\mathrm{Na}}) \tag{2.2}$$

$$I_{\mathrm{NaP\text{-}h}} = g_{\mathrm{NaP\text{-}h}} m_{\infty}(V) h (V - E_{\mathrm{Na}}) \tag{2.3}$$

$$I_{\mathrm{K}} = g_{\mathrm{K}} n^{4}(V - E_{\mathrm{K}}) \tag{2.4}$$

$$I_{\mathrm{Leak}} = g_{\mathrm{L}}(V - E_{\mathrm{L}}), \tag{2.5}$$

where the two gating variables n and h evolve according to

$$\frac{dx}{dt} = \frac{x_{\infty}(V) - x}{\tau_x(V)} \tag{2.6}$$

$$x_{\infty}(V) = \frac{1}{1 + \exp\frac{V - \Theta_x}{\sigma_x}} \tag{2.7}$$

$$\tau_x(V) = \frac{\bar{\tau}_x}{\cosh\frac{V - \Theta_x}{2\sigma_x}}, \tag{2.8}$$

where x represents the gating variable n or h.

This model assumes two simplifications in the fast Na^+ current I_{Na}. It is assumed m activates sufficiently fast to be considered instantaneous. Also, the time course of h is assumed to be approximated by $h = 1 - n$. In this model, bursting arises via fast activation and slow inactivation of a persistent Na^+ current, $I_{\mathrm{NaP\text{-}h}}$. Parameter values were chosen for bursting behavior and are given in appendix A.

Our goal was to construct a hybridized IF model that contains only the nonspiking currents $I_{\mathrm{NaP\text{-}h}}$, I_{L}, and I_{app} but captures temporal characteristics of the full model that result from interactions between the fast and slow subsystem.

3 Model Analysis

We first reframed the full model with the slow variable h treated as a parameter. We call this the FAST subsystem. Using the software XPPAUT (Ermentrout, 2002), we generated the bifurcation diagram for this system, graphing V versus h.

Bifurcation diagrams that characterize membrane voltage as a function of a slow gating variable have been used to classify oscillatory bursting phenomena for over a decade (Rinzel, 1985, 1987; Bertram, Butte, Kiemel, & Sherman, 1995; Izhikevich, 2000). In this type of analysis, we take advantage of the fact that bursting behavior is generated by the evolution of subsystems on two distinct timescales. This enables us to treat the slowly evolving variable as a parameter (i.e., quasi-steady-state) when studying the dynamics of the faster process. A bifurcation diagram is a plot of the steady-state voltage of the fast subsystem versus the "slow variable" parameter. This steady-state voltage may be stable or unstable, periodic or fixed, singular or multivalued. The manner in which these different solutions appear and disappear is carefully characterized, and the parameter value at which the transition occurs is called a bifurcation point. Bursting occurs for values of the slow variable that allow for regular transitions between stable fixed and periodic solutions. Bursting can then be characterized by the types of bifurcations that mediate these transitions (Izhikevich, 2000).

Square-wave bursting is phenomenologically characterized by a monotonically decreasing spike frequency and a burst envelope that rides on a plateau voltage without any undershoot. The fast subsystem is bistable and can be reset by a brief perturbation (Rinzel, 1985, 1987; Izhikevich, 2000). This type of bursting begins at a saddle-node (SN) bifurcation and ends at a saddle-loop bifurcation. Figure 1 illustrates bursting generated by the Butera model of bursting respiratory neurons in the pre-Bötzinger complex of the mammalian medulla (Butera et al., 1999a). Figure 2A is the corresponding bifurcation diagram of the membrane voltage of the reduced FAST subsystem with slow gating variable h treated as a parameter.

On the S-shaped curve of the solution manifold in Figure 2A, stable fixed points are represented by a solid line and unstable fixed points by a dotted line. The maxima and minima of periodic orbits are shown, as well as the h nullcline ($dh/dt = 0$) of the full model. Filled circles depict stable periodic solutions, and open circles depict unstable orbits. In Figure 2B, a detail of the bifurcation diagram includes a burst cycle $V(h)$.

An SN bifurcation is a point where a stable equilibrium solution and an unstable equilibrium solution coalesce and disappear. Periodic solutions arise at a Hopf bifurcation. It can be seen in Figure 2B that the trace of the burst cycle oscillates between the hyperpolarized equilibrium branch and the depolarized periodic solution branch. On the periodic solution branch, $dh/dt < 0$, and the trajectory moves to the left (with decreasing spike frequency) until it "falls off" the periodic solutions branch onto the stable

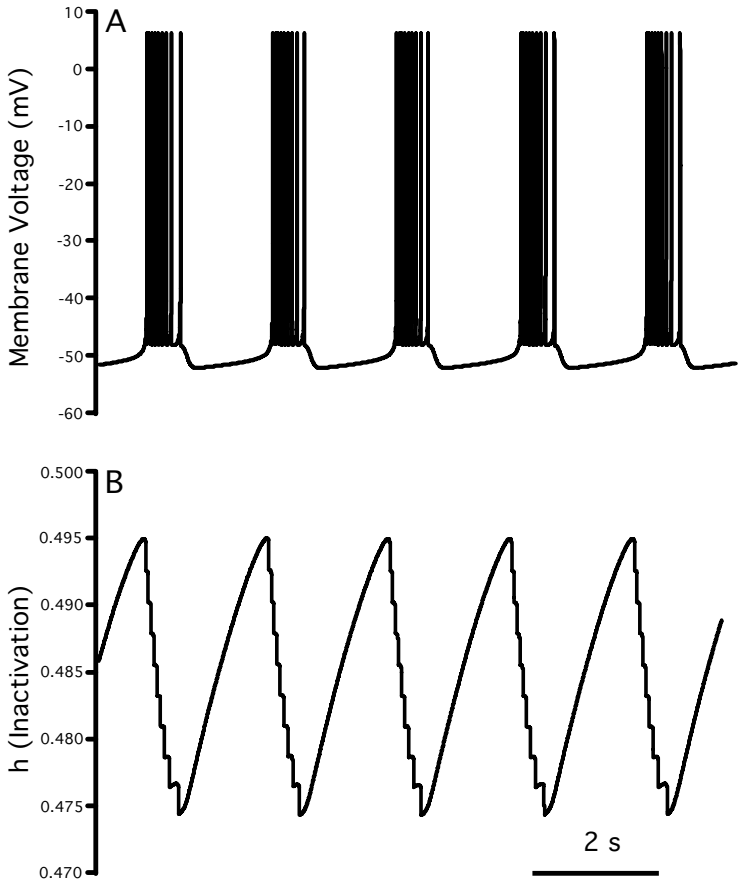

Figure 1: Time series of Butera model of bursting neurons in the pre-Bötzinger complex, $I_{app} = 20$ pA. (A) Membrane voltage V versus time. (B) Inactivation variable h versus time. See appendix A for parameter value details.

equilibrium branch. On this branch, $dh/dt > 0$, and the trajectory moves to the right. The membrane potential gradually increases until the equilibrium solution disappears at the SN bifurcation and the trajectory jumps up to the periodic solution branch. At this point, the cycle repeats itself.

4 Model Hybridization

Previously, Hansel and Mato (2003) fit an experimentally obtained current-frequency plot to a quadratic IF model. Our approach starts from a similar perspective, fitting one of our model parameters to reproduce the h-

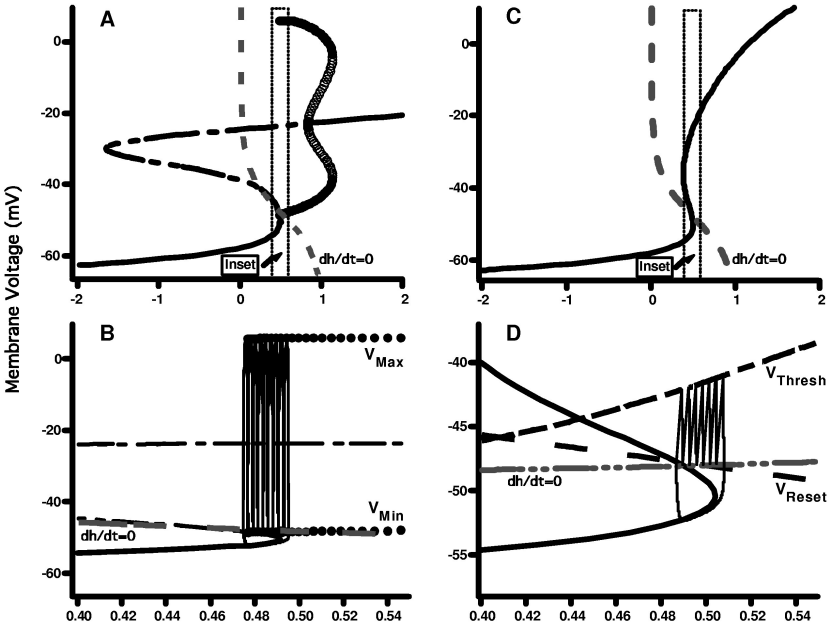

Figure 2: Bifurcation diagrams of the full and hybrid models. (A,B): The FAST subsystem of the full model. (A) Membrane voltage V versus inactivation variable h treated as a parameter. The nullcline $dh/dt = 0$ is shown as a dashed line. Stable fixed points of the FAST subsystem are represented by a solid line and unstable fixed points by a dashed-dotted line. Filled circles depict stable periodic solutions, and open circles depict unstable periodic solutions of the FAST susbystem. (B) Detail including a burst cycle V versus h for $I_{\text{app}} = 20$ pA. V_{Max} and V_{Min} are determined by the upper and lower branches of the stable periodic solutions. (C,D): The FAST subsystem of the hybrid model. (C) Membrane voltage V versus inactivation variable h treated as a parameter. The nullcline $dh/dt = 0$ is shown as a dashed line. There are no periodic solutions. (D) Detail including a burst cycle V versus h for $I_{\text{app}} = 20$ pA. $V_{\text{Thresh}}(h)$ and $V_{\text{Reset}}(h)$ are shown as dashed lines.

frequency plot of the full model. We then extend this analysis to consider the effects of individual spikes on the slow gating variable h.

The lower arm of the periodic solutions branch of the solution manifold consists of the minimum voltages of these solutions. Figure 3A shows this detail with a quadratic fit superimposed, defined as $V_{\text{Reset}}(h)$. This function gives the value to which the membrane voltage must be reset after every spike. It is used as V_{Reset} in our hybrid IF model.

The spike frequencies f for specific values of h are available from the analysis that produces the periodic solutions manifold. Using an IF model

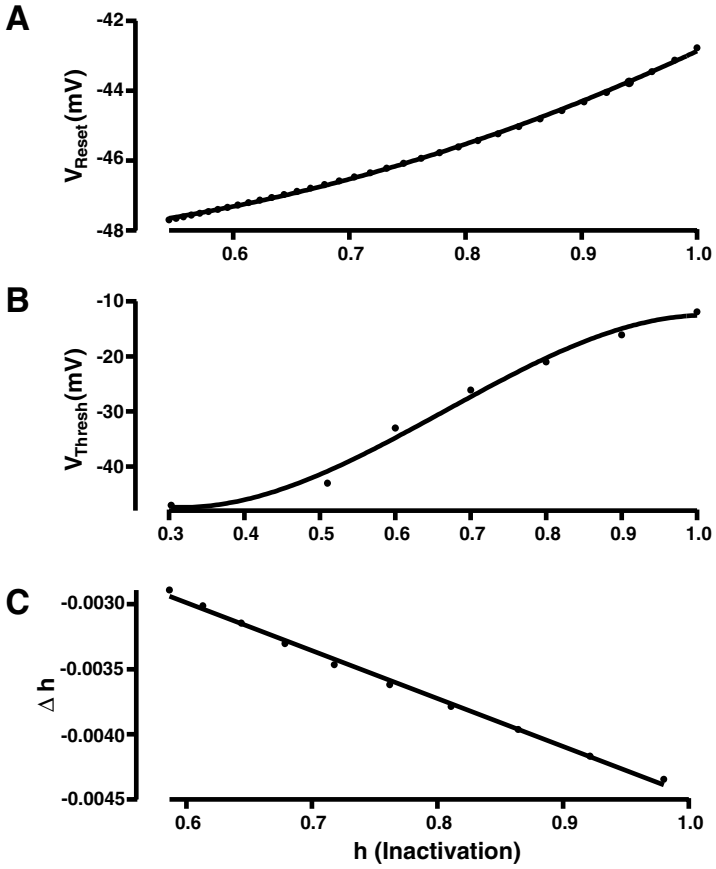

Figure 3: Interaction functions for the hybrid IF model. (A) V_{Reset} versus h. This function provides the value to which the membrane voltage is reset after a spike event. (B) V_{Thresh} versus h. This function determines the value of V at which a spike event is declared to have occurred. (C) Δh versus h. This function is invoked at each spike event to incorporate the effect of the action potential on the inactivation variable.

of the form

$$C\frac{dV}{dt} = -I_{\text{NaP-h}} - I_{\text{L}} + I_{\text{app}} \tag{4.1}$$

with h as a parameter and $V_{\text{Reset}}(h)$ already defined above, we computed the values of $V_{\text{Thresh}}(h)$ necessary to reproduce this *h-f* plot at a nominal value of I_{app} (see Section 6.). Figure 3B shows these values graphed versus h

with a third-order polynomial fit, $V_{\text{Thresh}}(h)$, superimposed. This function is used as V_{Thresh} in our model. It provides the membrane voltage at which a "spike event" is declared to have occurred, after which the system is reset to $V_{\text{Reset}}(h)$.

The perturbation of the slow variable by the voltages of the action potential is nontrivial in the evolution of the burst cycle. Figure 1B details the dynamic behavior of h. The firing of each action potential during the burst perturbs the inactivation variable h in the negative direction, pushing the model toward its silent state. To incorporate this effect into our reduced model, we turned our attention to the actual change in h during the burst cycle. Using data from XPPAUT, we isolated the trace of one period of the membrane voltage, V versus t, for given values of h. This waveform is referred to as $V(t; h)$, and it has period $T(h)$. We then integrated dh/dt for a given value of $h = \bar{h}$ over the period $T(\bar{h})$ according to

$$\begin{aligned}\Delta h(\bar{h}) &= \int_0^{T(\bar{h})} \frac{dh}{dt}\,\mathrm{d}t \\ &= \int_0^{T(\bar{h})} \frac{h_\infty\left(V(t,\bar{h})\right) - \bar{h}}{\tau_h\left(V(t,\bar{h})\right)}\,\mathrm{d}t. \end{aligned} \tag{4.2}$$

Consequently $\Delta h(\bar{h})$ describes the perturbation of h by an action potential over a single action potential period. Figure 3C shows these values graphed versus h with a linear fit superimposed. We use this function, $\Delta h(h)$, in our model to perturb the value of h after a spike event in the same manner as the voltage of an action potential would perturb h in the full model.

The resulting model numerically integrates only two differential equations, dV/dt and dh/dt, with dV/dt modified to contain only the subthreshold (nonspiking) currents. The structure of an IF model is used to perturb this integration by declaring a "spike event" at the crossing of $V_{\text{Thresh}}(h)$, whereupon $V(t)$ is reset by $V_{\text{Reset}}(h)$ and $h(t)$ is reset by $\Delta h(h)$. $V_{\text{Thresh}}(h)$ forces the model to have physiologically relevant spike frequency characteristics. $V_{\text{Reset}}(h)$ correlates the minimum voltage during spiking in the reduced model to those in the full model. The perturbation of the slow variable h by the action potentials (see Figure 1B) is accomplished with $\Delta h(h)$.

Thus, our hybrid IF model can be summarized:

$$\begin{aligned} C\frac{dV}{dt} &= -I_{\text{NaP-h}} - I_{\text{L}} + I_{\text{app}} \\ \frac{dh}{dt} &= \frac{h_\infty(V) - h}{\tau_h(V)} \end{aligned}$$

when $V \geq V_{\text{Thresh}}(h)$,
{
$V = V_{\text{Reset}}(h)$
$h = h + \Delta h(h)$
}

with the auxiliary functions $h_\infty(V)$, $m_\infty(V)$, and $\tau_h(V)$ defined as in equations 2.7 and 2.8. The algebraic forms for $V_{\text{Reset}}(h)$, $V_{\text{Thresh}}(h)$, and $\Delta h(h)$ are given in appendix B.

5 Results

5.1 Model Comparison. We studied the hybrid IF model's response to the control parameter I_{app} across a broad range ($0 \leq I_{\text{app}} \leq 35$ pA) and compared it to the full model according to several criteria: (1) mode of activity (silence, bursting and tonic firing) and when bursting, (2) burst period, (3) number of spikes per burst, and (4) length of burst.

For the parameter values noted in appendix A, the hybrid model accurately reproduces the mode of activity of the full model. Figure 4 compares the full model to the hybrid model for four different values of I_{app}. Since the membrane voltage amplitudes have not been replicated, spike events in the hybrid model have been noted by vertical bars at $V = -20$ mV.

In addition, we tested the robustness of the hybrid model by varying another key parameter: the conductance of the persistent sodium current, $g_{\text{NaP-h}}$. The results are summarized in Figure 5. The two models differed slightly in the magnitude of $g_{\text{NaP-h}}$ necessary for the onset of both spiking and bursting behavior. The full model exhibits no spiking behavior until $g_{\text{NaP-h}} = 1.6$ nS. This threshold in the hybrid model is $g_{NaP\text{-}h} = 1.8$ nS. In the full model, we see bursting behavior for $g_{\text{NaP-h}} = 2.2$ nS, and in the hybrid model, this transition takes place at $g_{\text{NaP-h}} = 2.3$ nS. For values of $g_{\text{NaP-h}}$ greater than the threshold for bursting, the hybrid model continues to reproduce the mode of activity of the full model as $g_{\text{NaP-h}}$ is increased, although the transition from bursting to tonic firing becomes less correlated at values of $g_{\text{NaP-h}} \geq 4.0$ nS.

The criteria we evaluated for bursting activity are reported in Figure 6. The hybrid model is most successful in reproducing the burst period in the full model, as shown in Figure 6A. Although the hybrid model accurately models the change in number of spikes per burst as applied current varies—the two curves in Figure 6B are nearly parallel—the hybrid model consistently produces two to three fewer spikes per burst than the full model produces.

The hybrid model also generates bursts that are of somewhat shorter duration than the full model, as shown in Figure 6C. This is particularly true for $I_{\text{app}} > 18$ pA, a result not completely unexpected. Higher values of applied current move the full model into the transition from bursting to

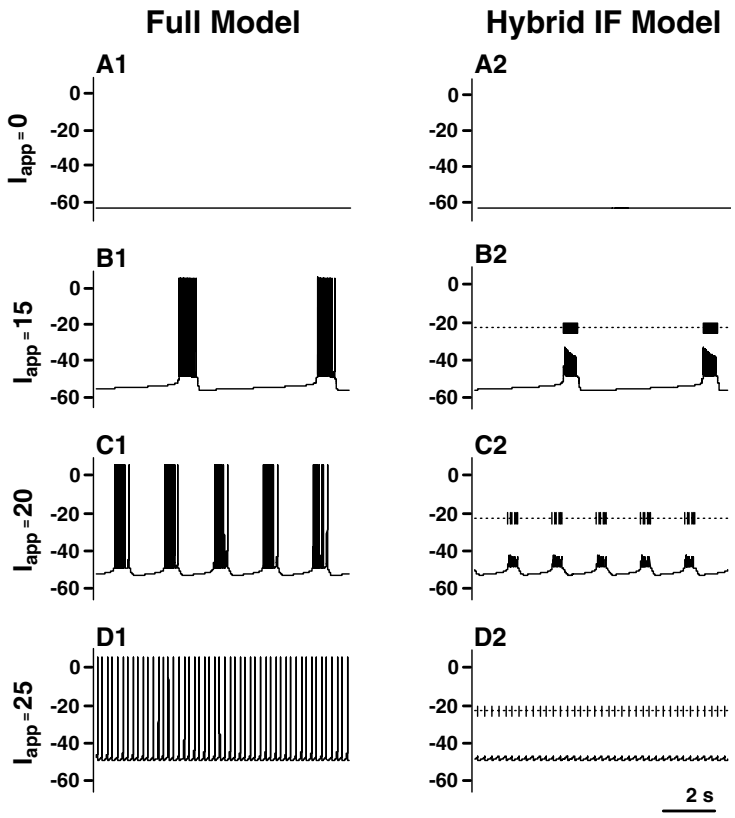

Figure 4: Comparison of dynamic response of both models as a function of applied stimulus. (A1/A2) $I_{app} = 0$, steady state. (B1/B2) $I_{app} = 15$ pA, bursting. (C1/C2) $I_{app} = 20$ pA, bursting. (D1/D2) $I_{app} = 25$ pA, tonic firing. Note that for clarity, spike events in the hybrid IF model (*B2, C2, D2*) are noted at $V = -20$ mV.

continuous spiking. In this transition, burst dynamics become more complex and often chaotic, and the mechanisms underlying this phenomena are well understood (Terman, 1992). The difficulty of collecting consistent data from the full model is reflected in the error bars added to Figure 6C for $I_{app} = 20$ pA and $I_{app} = 22$ pA. The less complex dynamics of the hybrid model prohibit it from exhibiting this phenomenon. When the range of data from the full model is compared with the hybrid model, we consider the two curves to be roughly parallel.

5.2 Computational Performance. As a final comparison of the two models, we timed computational runs, measuring the performance of the re-

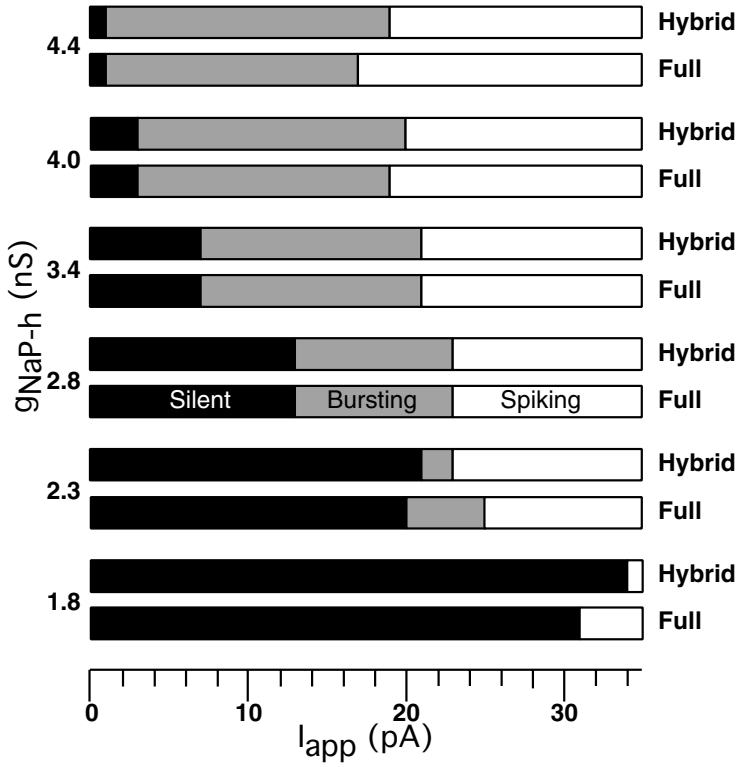

Figure 5: Comparison of dynamic response of both models as a function of $g_{\text{NaP-h}}$ and applied stimulus. The hybrid model is based on analysis of the full model for $g_{\text{NaP-h}} = 2.8$ nS.

duced and full model for both single neurons and networks across a range of applied current, $13 \leq I_{\text{app}} \leq 25$ pA. The parameter I_{app} was chosen since it biases the mode of cellular activity (see Figure 4). All timing runs were of equal length and given initial conditions already on the stable limit cycle. Simulation times were obtained using UNIX operating system calls that provide a measure of true CPU time of the running process. All file output was disabled so that the timing results were not contaminated by disk-writing overhead.

For our single-neuron timing runs, we implemented the full and reduced models in two ways: in the C programming language and in NEURON using the built-in CVODE integrator. For network simulations, we implemented the excitatory network model of Butera, Rinzel, and Smith (1999b), which consists of heterogeneous neurons all-to-all connected by excitatory AMPA synapses. We ran simulations consisting of 50 to 200 neurons and compared

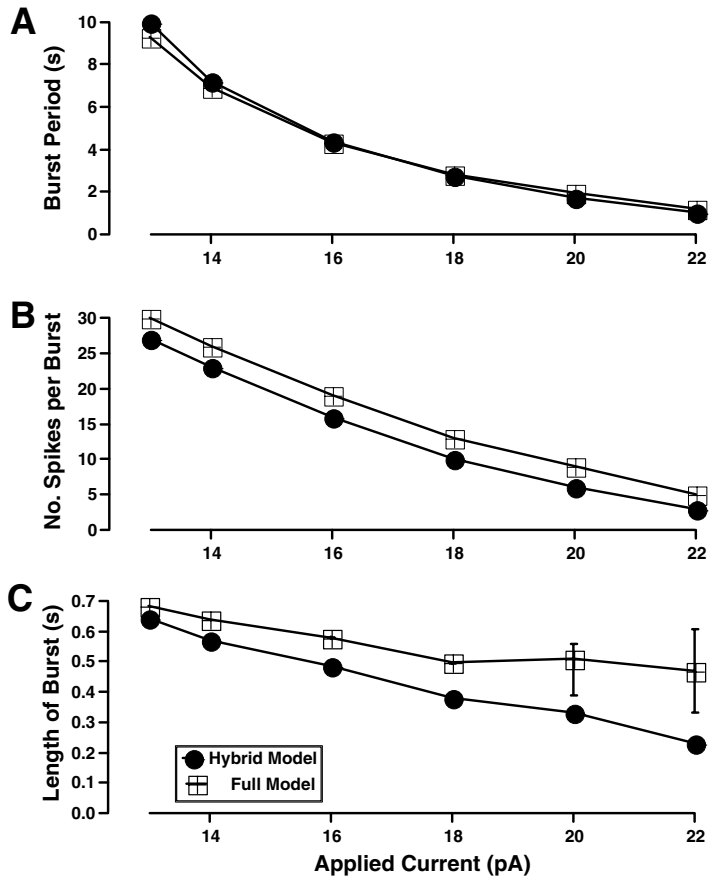

Figure 6: Comparison of burst characteristics of both models as a function of applied stimulus. (A) Burst period versus I_{app}. (B) Number of spikes per burst versus I_{app}. (C) Length of burst versus I_{app}. The full model is represented by open squares, the hybrid IF model by filled circles.

the process run time of the reduced model network and the full model network. Timings were made after start-up transients had died away and for the network simulating 60 seconds of network activity. As the size of the network increased, the conductance of each synapse was decreased to maintain networks with similar mean levels of overall synaptic input per cell and similar overall dynamics independent of n. These comparisons were done for three values of I_{app} corresponding to three different modes of activity: slow bursting, fast bursting, and tonic spiking. Varying I_{app} in

the network simulations is algebraically analogous to varying the leakage reversal potential E_L in the simulations of Butera et al. (1999b).

Results are summarized in Figure 7A. The C version of the single-neuron model was faster than the NEURON implementation not only because it was written in C, but because the detection of threshold crossings was implemented by an "if" statement and not by rigorously computing the exact time of threshold crossing, as is done in NEURON.

The results of Figure 7A show that while a speedup of 15-fold or more is obtained when simulating single cells for all values of I_{app}, the speedup decreases as a function of network size, with a lowest speedup of 3.9 for $n = 200$ cells.

We investigated to what extent the use of our reduced model was responsible for this reduction in speedup. Although the reduced model is clearly simpler, the added complexity of finding the times of crossings of V_{thresh} may not simply scale linearly with the size of the network for a network simulation. Another potential cause for the reduction of speedup is the larger number of synaptic events that NEURON must process for larger and larger networks. To address these issues, we ran simulations for the full and reduced model, for both $p = 1$ and $p = 0.1$, and for n = 50, 200, 500, and 1000, where n is the number of neurons in the network and p is the probability of a connection. When $p = 0.1$, the conductance of each synapse was increased by $1/p$ to maintain similar network dynamics for comparable benchmarking. For these simulations, E_L (a parameter in Butera et al., 1999b, that controls network excitability) was set to -60 mV, similar to setting I_{app} = 14 pA in the earlier results. For these simulations, the speedup as a function of n is illustrated in Figure 7B. Similar results were obtained for $p = 0.1$ (not shown).

To analyze the performance data as a function of p and n, we made the following assumptions:

1. There is a fixed cost for processing a synaptic event, and the amount of time devoted to solving synaptic events scales with $pn(n-1)$.
2. The time spent numerically integrating the intrinsic cell models scales with $O(n^x)$, where $x \geq 1$. This is based on numerical linear algebra assumptions. The computational complexity of solving a set of m differential equations is of $O(m^2)$ but can be as low as $O(m)$ if all the equations are independent of one another. The independence of individual cell models and the "local dt" option in NEURON may make the computation time scale with $O(n)$. Conversely, larger numbers of synaptic inputs create more events and thus more time steps to be solved per cell, and both the number of synaptic events as well as a worst-case numerical integrator scales with $O(n^2)$.

If $x < 2$ and n becomes arbitrarily large, we would expect the computation time to scale with n^2. If this were to occur, it suggests that for large

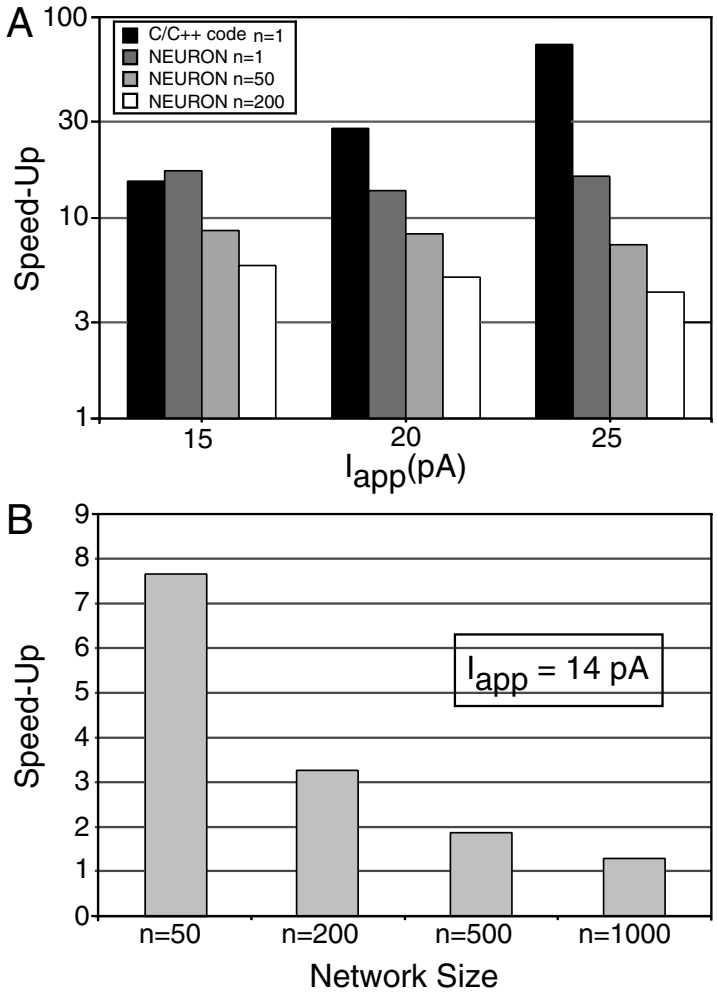

Figure 7: Computational performance (A) Speedup of hybrid versus full model. For $n = 1$, there are two implementations: a fourth-order stiff integrator in the C programming language and the internal CVODE integrator in the NEURON simulation environment. Heterogeneous excitatory networks of $n = 50$ and $n = 200$ were also implemented in NEURON. See the text for details. (B) Speedup of full versus hybrid network as a function of network size. All data were taken for $E_L = -60$mV, equivalent to $I_{app} = 14$pA.

n, the overhead in processing synaptic events is the dominant effect on computation time. A plot of computation time versus n on a log-log scale (not shown) reveals a slope of approximately 2 for the reduced model and about 1.5 for the full model. If we assume that the reduced model is of less computational complexity than the full model, this result suggests that the overhead associated with processing synaptic events is responsible for the reduced speedup for large n.

To investigate this issue further, we used the Nelder-Meld simplex method to identify parameters for the following formulation, choosing parameters that minimize the log error between the formula and the data points, with an additional constraint that $x \geq 1$:

$$T(n) = K_i n^x + K_s p n(n-1), \tag{5.1}$$

where K_i represents the computational overhead for solving the dynamic equations for a single cell and K_s represents the computational overhead for handing a single synaptic event. Our best-fit results are set out in Table 1. Although we did not impose such a constraint, we would expect that the K_s values would be similar for the full and reduced model, since NEURON processes both identically. In practice, the estimated parameters were within 25% of each other. The estimate also suggests that K_i is much less for the reduced model, which is to be expected due to its lower computational complexity for a single cell. Finally, it shows that x is about 1.86 for the reduced model and 1.27 for the full model. From these estimates, we conclude that:

1. While the reduced model is much faster for a single cell (speedup results and lower K_i), for a network its computational complexity scales greater with n than the full model, somewhat limiting speedup for network simulations.
2. Since $x < 2$, the overhead processing synaptic events ultimately becomes the limiting factor affecting the computation time of large network simulations.

We make these conclusions with several caveats. They are merely based on fits to performance timings of a single simulation, and there are many model- and simulator-dependent factors and parameters that can affect these re-

Table 1: Fit of Performance Timing Data for Reduced and Full Model to Parameters of Equation 5.1.

Model	K_i (sec)	x (unitless)	K_s (sec)
Reduced	0.0902	1.8577	0.0097
Full	7.614	1.2669	0.0122

sults. They were also benchmarked for one particular simulation with a particular mode of activity (network wide bursts separated by periods of silence), which will also affect timing results (see Figure 7A for single cell examples).

In summary, we conclude that although the reduced model is much faster than the full model for a single cell, its computational complexity scales more with n than the full model, leading to reduced speedup for larger simulations. Furthermore, the overhead in processing synaptic events for large networks makes the speedup gains for any reduced-cell model negligible for n much greater than 1000. Thus, our reduced model formulation is most effective in gaining speedup for networks of $n \leq 500$ in particular, and networks of fewer than 1000 neurons in general.

6 Discussion

We have described a reduction of an HH-style bursting neuron to a hybridized IF formalism based on a thorough bifurcation analysis of the neuron's dynamics. The reduced model successfully reproduces characteristic behavior and temporal attributes of the full model across a physiologically relevant range of applied current stimulus. This complexity is achieved by incorporating both the effect of the action potential on the slow variable and the effects of the slow variable on the subthreshold membrane dynamics that ultimately regulate the generation of action potentials.

The hybrid IF model has only one timescale: that of the slow variable. The absence of spiking currents, combined with contemporary variable time-step algorithms, results in potentially significant savings in computational time. The model holds promise for large-scale simulation of coupled bursting systems (Butera et al., 1999b).

A limit of this approach is that our reduction is formally constrained to those parameters that were studied in the numerical bifurcation analysis used to derive the hybrid model. In fact, although our analysis was performed for a fixed value of I_{app} and $g_{\text{NaP-h}}$, we were surprised to find that the dynamics of the hybrid and full model were quite comparable across a range of values for both parameters.

For values of $g_{\text{NaP-h}}$ below the bursting threshold, the hybrid model does not adequately reproduce the transition from silence to spiking. Since our construction of the model was drawn from analysis done exclusively on the bifurcation diagram of the full model in bursting mode, we did not expect the reduced model to reproduce these dynamics.

For values of $g_{\text{NaP-h}}$ above the bursting threshold, the transition from silence to bursting is accurately reproduced. This transition in the full model is primarily modulated by increasing activation of the subthreshold currents. Since these currents are fully represented in the hybrid model, the high correlation of this transition threshold is not unexpected. At higher values of $g_{\text{NaP-h}}$, the transition from bursting to spiking becomes slightly

less correlated between the two models. In the full model, this transition is more intricate, involving the activated I_{Na} and I_K as well as their interactions with the slowly inactivating $I_{NaP\text{-}h}$. The reduced model does not incorporate this complexity and is not intended to do so in its present form.

We note also that the auxiliary functions are algebraic fits for data points acquired in the physiological range of h and are valid only in that range—approximately $0.3 < h < 1$. To give one example, the model as presented could never exhibit depolarization block for a large current injection. Not only are the ranges of I_{app} that induce depolarization block beyond normal physiological range, but since our action potentials are threshold detected, V_{Thresh} is always greater than V_{Reset}. An effect analogous to depolarization block could occur if the functions were reformulated to allow for a range of h where V_{Reset} is greater than V_{Thresh}. We have developed variants of our model where this occurs, and as long as the voltage nullcline has a stable solution as a function of h where $V > V_{Reset}(h)$, then depolarization block does indeed occur.

A more thorough reduction of our model would incorporate the effects of the ionic conductances and I_{app} on V_{Reset}, V_{Thresh} and Δh. This would allow better comparison of dynamical behavior, resulting in variations of other parameters such as conductances that are targets of neuromodulators or synaptic transmission.

Our computational analysis reveals that for a large-scale neural network simulation, the implementation of faster models is but one factor in achieving speedup in network simulations. Although speedup occurs for networks as large as $n = 1000$, other factors, such as overhead in solving for synaptic events, which scale with n^2 for a network of size n, must also be considered.

Appendix A

Parameters for the Butera model of pre-Bötzinger bursting neurons (units are mV, nS, pF, pA, and ms) are as follows:

$$\begin{aligned} E_K &= -85 \\ E_{Na} &= 50 \\ E_L &= -65 \\ g_K &= 11.2 \\ g_{Na} &= 28 \\ g_{NaP\text{-}h} &= 2.8 \\ g_L &= 2.8 \\ c &= 21 \\ \Theta_{m\text{-}Na} &= -34 \\ \Theta_{m\text{-}NaPh} &= -40 \end{aligned}$$

$$
\begin{aligned}
\Theta_h &= -48 \\
\Theta_n &= -29 \\
\sigma_{m\text{-Na}} &= -5 \\
\sigma_{m\text{-NaPh}} &= -6 \\
\sigma_h &= 6 \\
\sigma_n &= -4 \\
\bar{\tau}_h &= 10,000 \\
\bar{\tau}_n &= 10 \\
13 \leq I_{\text{app}} &\leq 25 \\
v(0) &= -53 \\
h(0) &= 0.6 \\
n(0) &= 0.003
\end{aligned}
$$

Appendix B

Functions used in the hybrid IF model:

$$V_{\text{Reset}}(h) = -47.359 - 6.5825h + 11.085h^2 \tag{B.1}$$

$$V_{\text{Thresh}}(h) = -18.8970 - 200.41h + 414.62h^2 - 207.88h^3 \tag{B.2}$$

$$\Delta h(h) = -0.00078 - 0.0037h \tag{B.3}$$

Acknowledgments

This work was supported by a grant from the National Institutes of Health (R01-MH62057) to R.J.B. We thank William Lytton and Michael Hines for assistance in implementing the threshold-based model in NEURON.

References

Baer, S., Rinzel, J., & Carillo, H. (1995). Analysis of an autonomous phase model for neuronal parabolic bursting. *Journal of Mathematical Biology, 33*, 309–333.

Bertram, R. (1993). A computational study of the effects of serotonin on a molluscan burster neuron. *Biological Cybernetics, 69*, 257–267.

Bertram, R., Butte, M., Kiemel, T., & Sherman, A. (1995). Topological and phenomenological classification of bursting oscillations. *Bulletin of Mathematical Biology, 57*, 413–439.

Butera, R., Clark, J., & Byrne, J. (1996). Dissection and reduction of a modeled bursting neuron. *Journal of Computational Neuroscience, 3*, 199–223.

Butera, R., Clark, J., & Byrne, J. (1997). Transient responses of a modeled bursting neuron: Analysis with equilibrium and averaged nullclines. *Biological Cybernetics, 77*, 307–322.

Butera, R., Clark, J., Canavier, C., Baxter, D., & Byrne, J. (1995). Analysis of the effects of modulatory agents on a modeled bursting neuron: Dynamic interactions between voltage and calcium dependent systems. *Journal of Computational Neuroscience, 2*, 19–44.

Butera, R., Rinzel, J., & Smith, J. (1999a). Models of respiratory rhythm generation in the pre-Bötzinger complex. I. Bursting pacemaker neurons. *Journal of Neurophysiology, 82*, 382–397.

Butera, R., Rinzel, J., & Smith, J. (1999b). Models of respiratory rhythm generation in the pre-Bötzinger complex. II. Populations of coupled pacemakers. *Journal of Neurophysiology, 82*, 398–415.

Canavier, C., Clark, J., & Byrne, J. (1991). Simulation of the bursting activity of neuron R15 in *Aplysia*: Role of ionic currents, calcium balance, and modulatory transmitters. *Journal of Neurophysiology, 66*, 2107–2124.

Destexhe, A. (1997). Conductance-based integrate and fire models. *Neural Computation, 9*, 503–514.

Ermentrout, G. (1994). Reduction of conductance-based models with slow synapses to neural nets. *Neural Computation, 6*, 679–695.

Ermentrout, G. (2002). *Simulating, analyzing, and animating dynamical systems: A guide to XPPAUT for researchers and students*. Philadelphia: Society for Industrial and Applied Mathematics.

Hansel, D., & Mato, G. (2003). Asynchronous states and the emergence of synchrony in large networks of interacting excitatory and inhibitory neurons. *Neural Computation, 15*, 1–56.

Hines, M., & Carnevale, N. (1997). The NEURON simulation environment. *Neural Computation, 9*, 1179–1209.

Hines, M., & Carnevale, N. (2000). Expanding NEURON's repertoire of mechanisms with nmodl. *Neural Computation, 12*, 995–1007.

Izhikevich, E. (2000). Neural excitability, spiking, and bursting. *International Journal of Bifurcation and Chaos, 10*, 1171–1266.

Kepler, T., Abbott, L., & Marder, E. (1992). Reduction of conductance-based neuron models. *Biological Cybernetics, 66*, 381–387.

Koch, C. (1999). *Biophysics of computation.* New York: Oxford University Press.

Lapicque, L. (1907). Recherches quantitatives sur l'excitation électrique des nerfs traitée comme une polarization. *Journal of Physiology (Paris), 9*, 620–635.

MacGregor, R. J. (1987). *Neural and brain modeling*. San Diego, CA: Academic Press.

Press, W., Flannery, B., Teukolsky, S., & Vetterling, W. (1992). *Numerical recipes in C* (2nd ed.). Cambridge: Cambridge University Press.

Rinzel, J. (1985). Bursting oscillations in an excitable membrane model. In B. Sleeman & D. Jones (Eds.), *Lecture notes in mathematics* (Vol. 1151). Berlin: Springer-Verlag.

Rinzel, J. (1987). A formal classification of bursting mechanisms in excitable systems. In E. Teramoto & M. Yamaguti, (Eds.), *Lecture notes in biomathematics* (Vol. 71, pp. 267–281). Berlin: Springer-Verlag.

Rinzel, J., & Lee, Y. (1987). Dissection of a model for neuronal parabolic bursting. *Journal of Mathematical Biology, 25*, 653–675.

Smith, G., Cox, C., Sherman, S. M., & Rinzel, J. (2000). Fourier analysis of sinusoidally driven thalamocortical relay neurons and a minimal integrate-and-fire-or-burst model. *Journal of Neurophysiology, 83*, 588–610.

Smolen, P., Terman, D., & Rinzel, J. (1993). Properties of a bursting model with two slow inhibitory variables. *SIAM Journal of Applied Mathematics, 53*, 861–892.

Terman, D. (1992). The transition from bursting to continuous spiking in excitable membrane models. *Journal of Nonlinear Science, 2*, 135–182.

Received January 8, 2003; accepted June 3, 2003.